Stepwise Synthesis and Structure Analysis of Mo Dimers in NaY Zeolite

Kiyotaka Asakura,[†] Yoshiaki Noguchi,[‡] and Yasuhiro Iwasawa*[,‡]

Research Center for Spectrochemistry, and Department of Chemistry, Graduate School of Science, the University of Tokyo, Hongo, Bunkyo-ku, Tokyo 113-0033, Japan

Received: August 11, 1998; In Final Form: October 14, 1998

Mo dimers were prepared in the supercage of NaY zeolite by cycles of saturated adsorption of $Mo(CO)_6$ at room temperature and subsequent thermal decomposition at 573 K. The obtained samples were characterized by temperature-programmed desorption, extended X-ray absorption fine structure (EXAFS), X-ray photoelectron spectra, and X-ray fluorescence. Two $Mo(CO)_6$ molecules per supercage were immobilized in each process. After the thermal decomposition of the adsorbed $Mo(CO)_6$ in the supercage, the resultant Mo(1)/NaY could accept two more $Mo(CO)_6$ molecules per supercage. Mo loading was found to increase linearly by two $Mo(CO)_6$ molecules in a supercage per one deposition cycle, and was saturated with eight Mo atoms per supercage after the four cycles. EXAFS analysis revealed that Mo(II) oxocarbide dimer species $[Mo_2(C)(O)_x]$ with the Mo−Mo distance of 0.285 nm was formed in the supercage by the 573 K thermal decomposition of the adsorbed $Mo(CO)_6$. The structures of Mo oxocarbide dimers were invariant regardless of the Mo loading.

Introduction

Zeolites as crystalline microporous materials provide nanospaces for syntheses of active catalytic materials.[1] Nanosize metal particles, organometallic complexes, and clusters have been prepared in the pore using the reaction of the metal ions and organic ligands called "ship-in-bottle synthesis".[2−8] Active metal sites have also been prepared by repeated adsorption−decomposition cycles of suitable metal carbonyl precursors. $Mo(CO)_6$ can be immobilized in the 1.2-nm supercages of NaY zeolite by chemical vapor deposition(CVD).[9−28] Previous works indicate that the adsorption of $Mo(CO)_6$ occurs homogeneously and is saturated at two molecules per supercage owing to its size restriction [about 16 $Mo(CO)_6$ per unit cell].[13,19,20,25] Further deposition of $Mo(CO)_6$ becomes possible when the decarbonylation of the immobilized $Mo(CO)_6$ creates empty space. Ozin et al. reported that the $Mo(CO)_6$ in the cage was converted to $(MoO_3)_x$ clusters by photooxidation and further CVD process of $Mo(CO)_6$ was possible[19−21,25] with a gradual increase in the Mo amount up to four MoO_3 per supercage. Yong and Howe performed thermal decomposition of $Mo(CO)_6$ in NaY zeolite at 673 K, which made empty space for further $Mo(CO)_6$ adsorption and they found about 20 Mo in a supercage by 14 times adsorption−thermal decomposition cycles.[13] In this case the Mo species migrated during the thermal decomposition process at 673 K, which was demonstrated by extended X-ray absorption fine structure (EXAFS),[17] leading to inhomogeneous distribution of Mo species in such a manner that some pores contained Mo clusters and others remained empty. On the other hand, decomposition of $Mo(CO)_6$ in NaY supercages at lower temperature such as 473 K can produce Mo_2 species without undesired migration,[17] suggesting that the lower temperature decomposition of $Mo(CO)_6$ would produce Mo clusters with definite size that might distribute homogeneously in the NaY.

In this paper we investigated the behavior and structure of Mo species prepared by the deposition and subsequent thermal decomposition processes of $Mo(CO)_6$ in NaY at 573 K to provide an example of a stepwise synthesis of homogeneous Mo species in supercages.

Experimental Section

Preparation. NaY zeolite, obtained from Toso (HSZ-300NAA), contained 51 Al per unit cell (Si/Al = 2.6). $Mo(CO)_6$ was purchased from Aldrich (>98% purity). The zeolite was pretreated under high vacuum (10^{-3} Pa) at 723 K for 15 min and calcined at the same temperature under 26.6 kPa of oxygen for 30 min, followed by evacuation at 723 K for 1 h in a closed circulating system. Then the zeolite was set in a glass-made CVD apparatus without exposure to air. $Mo(CO)_6$ was placed in a glass tube connected to the CVD apparatus. To prevent photodecomposition of $Mo(CO)_6$, the $Mo(CO)_6$ tube reservoir was surrounded by Al foil. The whole apparatus was evacuated at 10^{-3} Pa and the NaY zeolite was exposed to $Mo(CO)_6$ vapor with stirring at room temperature. After the sufficient exposure time for saturation of $Mo(CO)_6$ adsorption in the zeolite pores (typically 15 h), the sample was evacuated at room temperature to remove the excess $Mo(CO)_6$. The color of the zeolite sample changed to pale yellow. The sample thus obtained was denoted as 1-$Mo(CO)_6$/NaY. The sample was then heated to 573 K at a heating rate of 4 K/min to remove all the CO ligands from the adsorbed Mo carbonyls; the sample was turned black by the thermal treatment. The process of saturated adsorption of $Mo(CO)_6$ and thermal treatment under vacuum at 573 K was repeated several times to obtain samples with various Mo loadings. The samples thus obtained are denoted as Mo(*n*)/NaY where *n* indicates the number of adsorption−thermal decomposition cycles.

For comparison, Mo/NaY samples were also prepared by an impregnation method using $(NH_4)_6Mo_7O_{24}$, followed by calcination at 673 K in air for 1 h. The samples are denoted as imp-Mo/NaY. The loading of Mo was 10 wt %, which corresponds to that of Mo(1)/NaY.

* Author for correspondence. Fax: 81-3-5800-6892; e-mail: iwasawa@chem.s.u-tokyo.ac.jp.

[†] Research Center for Spectrochemistry.

[‡] Department of Chemistry.

10.1021/jp983343g CCC: $18.00
Published on Web 01/30/1999

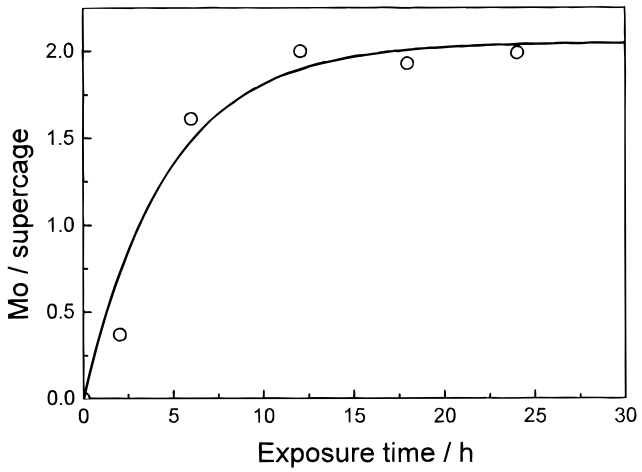

Figure 1. Time profile of $Mo(CO)_6$ adsorption at 298 K.

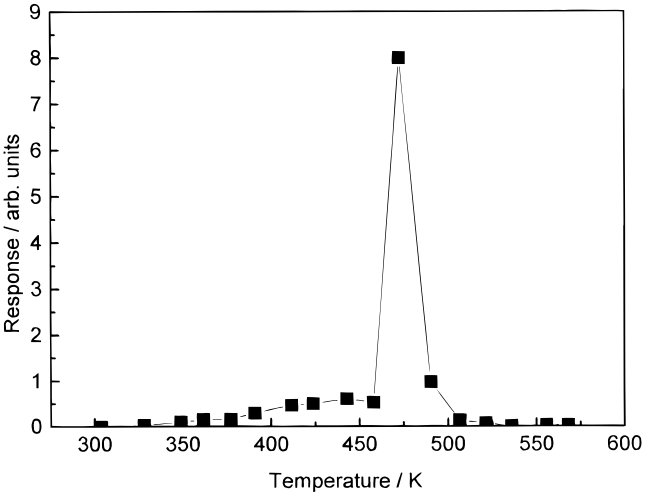

Figure 2. Temperature-programmed desorption spectra (TPD) of $Mo(CO)_6$ adsorbed on NaY. Heating rate: 4 K min^{-1}.

Characterization of the Catalysts. X-ray fluorescence (XRF) was measured on a SEA-2010 spectrometer (Seiko Electronic Industrial Co.) using an Rh target. Physical mixtures of MoO_3 and NaY with various ratios were used as references to estimate the loadings of Mo in the samples.

X-ray photoelectron spectra (XPS) were recorded on a Rigaku XPS-7000 (15 kV, 20 mA) using Mg Kα (1253.6 eV). The peak positions of XPS spectra were calibrated by Si $2p_{3/2}$ of NaY at 102.8 eV.[16] The samples were prepared in a closed circulating system and transferred to glass tubes. The samples were heated to 573 K under vacuum at a heating rate of 4 K/min. The glass tubes were sealed by glass-blowing and were carried into a N_2-filled plastic glove bag that was directly connected to an XPS entrance port. After the bag was evacuated and refilled with 99.99% N_2 three times, the glass tubes were opened in the bag and the samples were set on sample holders as quickly as possible.

Temperature-programmed desorption (TPD) experiments were carried out in a closed circulating system with a ramping speed of 4 K/min. The evolved gases in the TPD process were analyzed by a gas chromatograph using a Unibeads-C column, where the gases were evacuated for 10 s between the samplings. To measure a remaining carbon atom after the TPD process, the samples were oxidized with 26.6 kPa oxygen at 723 K for 30 min and the gas phase was analyzed by the gas chromatograph.

TABLE 1: Amounts of CO_2 Formed and Oxygen Consumed during the Oxidation of the TPD-Treated Samples

sample	CO_2/Mo	O_2/Mo	O uptake per Mo[a]
Mo(1)/NaY	0.5 ± 0.1	1.5 ± 0.2	2.0 ± 0.4
Mo(2)/NaY	0.4 ± 0.1	1.2 ± 0.2	1.6 ± 0.4
Mo(3)/NaY	0.4 ± 0.1	1.4 ± 0.2	2.0 ± 0.4

[a] O uptake per Mo = 2 × ((consumed O_2/Mo) − (produced CO_2/Mo)).

EXAFS spectra were measured at BL10B of the Photon Factory in the Institute of Materials Structure Science, High Energy Accelerator Research Organization (KEK−IMSS−PF). The electron storage ring was operated at 2.5 GeV-300 mA. Synchrotron radiation from the storage ring was monochromatized by a Si(311) channel cut crystal. Ionization chambers filled with $Ar-N_2$ = 1:1 mixed gas and Ar were used as detectors monitoring incident X-rays (I_0) and transmitted ones (I), respectively. The angle of the monochromator was calibrated by using Mo foil, the inflection point of which at the edge was set at 20 004 eV. The EXAFS samples were obtained by heating to 573 K with a ramping speed of 4 K/min under vacuum in a closed circulating system and transferred to EXAFS cells with Kapton windows without exposure to air. The EXAFS measurements were carried out at room temperature. To minimize the effect of higher harmonics, sample thickness was regulated for the μt to be less than 3. The EXAFS spectra were analyzed by EXAFS analysis program REX (Rigaku Co.) composed of background subtraction by cubic smoothing, Fourier transformation, and curve-fitting analysis.[29] The origin of photoelectron, E_0, was tentatively set at the inflection point of the absorption edge. The curve-fitting analysis was carried out using the following equations.

$$k^3\chi(k) = \sum_i k_i^2 N_i F_i(k) \exp(-2\sigma_i^2 k_i^2)\sin[2k_i r_i + \phi_i(k)]/r_i^2 \quad (1)$$

where N_i, r_i, and σ_i are coordination number, interatomic distance, and Debye−Waller factor for the ith shell, respectively. They were optimized during the curve-fitting procedure. $F_i(k)$ and $\phi_i(k)$ are amplitude and phase-shift functions, respectively. The reference compounds to extract the amplitude and phase-shift functions for Mo−Mo, Mo−C, and Mo−O were Mo foil, $Mo(CO)_6$, and K_2MoO_4, respectively. The E_0 was optimized for each shell using eq 2

$$k = \sqrt{k'^2 - \frac{2m}{\hbar^2}\Delta E_0} \quad (2)$$

The ranges of Fourier transformation and inverse Fourier transformation were 30−145 nm^{-1} and 0.1−0.35 nm, respectively. The number of independent parameters allowed for the fitting process given by $2\Delta k\Delta r/\pi+2$[30] was about 20 and the maximum number of the used fitting parameters was 12. The degree of the curve fitting was evaluated by the R_f factor defined as follows

$$R_f = \sqrt{\sum[(\chi_{obs}(k) - \chi_{cal}(k)]^2/\sum\chi_{obs}(k)^2} \quad (3)$$

Results

Adsorption Behavior of $Mo(CO)_6$. Figure 1 shows the amount of $Mo(CO)_6$ in a NaY zeolite against exposure time to $Mo(CO)_6$ vapor at room temperature, which was determined by means of XRF. The adsorption of $Mo(CO)_6$ was saturated at about 10 h, when the amount was 2 $Mo(CO)_6$ in a pore, agreeing with the literature.[12,13,20] Figure 2 shows TPD spectra

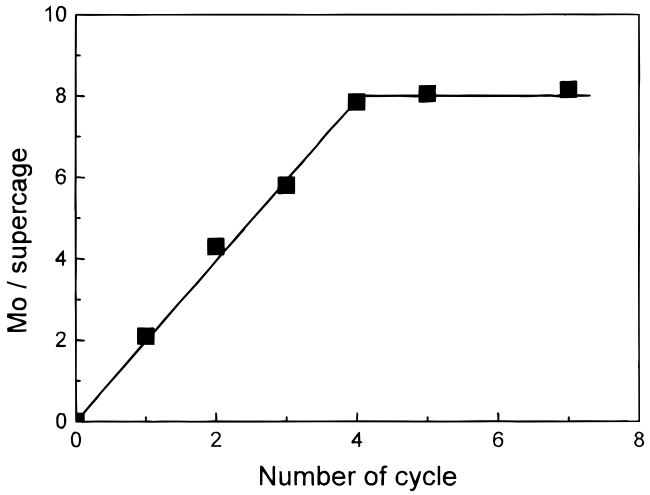

Figure 3. Number of Mo deposited per supercage as a function of number of the saturated adsorption/thermal decomposition cycle.

for CO from the sample [1-Mo(CO)$_6$/NaY], which was saturated with Mo(CO)$_6$ at room temperature. The desorption peak of CO appeared at 473 K and all CO desorption ceased at 573 K. Total amount of desorbed CO was about 5.5 per Mo without any CO_2 formation. To reduce the unfavorable aggregation of Mo, the decomposition of adsorbed Mo(CO)$_6$ was performed at 573 K. After the TPD measurement the Mo species was oxidized with O_2 at 673 K. One CO_2 per two Mo atoms was formed by the oxidation, as shown in Table 1, indicating that one carbon atom per two Mo atoms was left in the pores of NaY after the thermal treatment. Table 1 also shows the oxygen consumption in the oxidation process, where about two oxygen atoms were attached to one Mo atom.

Figure 3 shows the amount of Mo deposited on the NaY as a function of the number of saturated adsorption−thermal decomposition cycles. The Mo loading linearly increased up to four cycles, which corresponded to eight Mo atoms per supercage (64 Mo atoms per unit cell). The Mo loading did not increase by further deposition of Mo(CO)$_6$. Two Mo(CO)$_6$ molecules were charged per one cycle of the deposition process. However, the saturation amount of Mo was eight per supercage in this work. This result does not agree with the results of Yong and Howe et al.[13] and Ozin et al.,[20,25] who reported that the amount of Mo loading per one cycle did not linearly increase with the number of the deposition−decomposition cycles, though it gradually attained a saturation loading.

XPS Spectra. Figure 4 shows the Mo 3d XPS spectra for Mo(1)/NaY obtained by the Mo(CO)$_6$ deposition and subsequent thermal decomposition under vacuum at 573 K. Binding energies of Mo 3d$_{5/2}$ are summarized in Table 2. The Mo 3d$_{5/2}$ appeared at 228.8 eV for the Mo(1)/NaY sample. Mo 3d$_{5/2}$ peaks for Mo-(2)/NaY and Mo(3)/NaY appeared at similar binding energies, 228.7 and 228.8 eV, respectively. Figure 5 shows the plots of the intensity ratio of Mo 3d$_{5/2}$/Si 2p against the number of saturated adsorption−thermal decomposition cycles. The linear relation between them indicates that the Mo species are supported in a similar way at each adsorption−decomposition cycle. Figure 5 also shows the data point of Mo3d$_{5/2}$/Si2p for an imp-Mo(10 wt %)/NaY obtained by an impregnation method using aqueous solution of $(NH_4)_6Mo_7O_{24}$. The 10 wt % corresponds to Mo loading of the Mo(1)/NaY. It has been reported that Mo species are loaded on the external surface of NaY by the impregnation method, since the oxoanionic or neutral polymolybdates cannot enter the zeolite pores in the presence of water.[31,32] The peak intensity ratio, Mo 3d$_{5/2}$/Si2p,

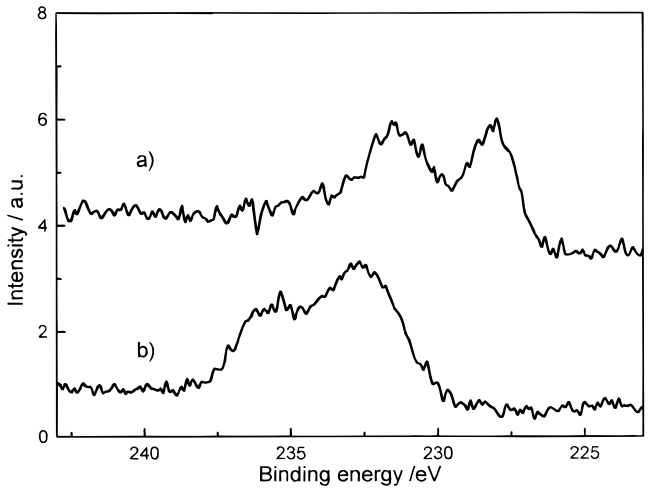

Figure 4. Mo 3d XPS spectra of Mo(1)/NaY (a) and imp-Mo(10 wt %)/NaY (b).

TABLE 2: Binding Energy of Mo3d$_{5/2}$ for Various Samples

	binding energy Mo 3d$_{5/2}$	reference
Mo(1)/NaY	228.8	this work
Mo(2)/NaY	228.7	this work
Mo(3)/NaY	228.8	this work
imp-Mo(10 wt %)/NaY	232.6	this work
1-Mo/NaY[a]	228.2	15
1-Mo/NaY[b]	228.4	15
1-Mo/NaY[c]	229.2	16
Mo(CO)$_6$	228.5	37
Mo	227.8−228.0	16
MoO_2	230.9	this work
MoO_3	232.9	this work
Na_2MoO_4	232.1	37
$Mo_2C_xO_y$[d]	228.58 (Mo−C) 232.2 (MoO_3)	38

[a] Treated at 473 K. [b] Treated at 633 K. [c] Treated at 673 K. [d] Partially oxidized molybdenum carbide bulk.

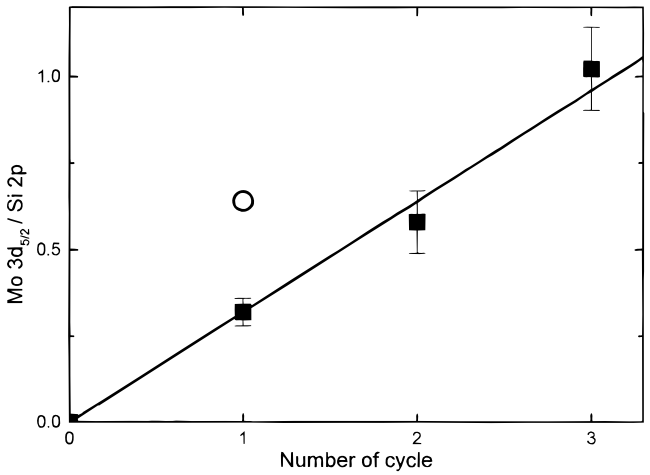

Figure 5. Intensity ratio Mo 3d$_{5/2}$/Si 2p in XPS spectra against the repeated cycles of the saturated adsorption/thermal decomposition (filled squares). The open circle is the intensity ratio of Mo 3d$_{5/2}$ to Si 2p for imp Mo(10 wt %)/NaY.

for Mo(1)/NaY was much smaller than that for the imp-Mo(10 wt %)/NaY, indicating the Mo species were located inside the zeolite.

EXAFS. Figure 6 shows EXAFS oscillations [$\chi(k)$] and the Fourier transforms of the $k^3\chi(k)$ for Mo(CO)$_6$ and 1-Mo(CO)$_6$/NaY. Peaks for Mo−C and Mo−O were observed around 0.16 and 0.28 nm, respectively, which were inversely Fourier

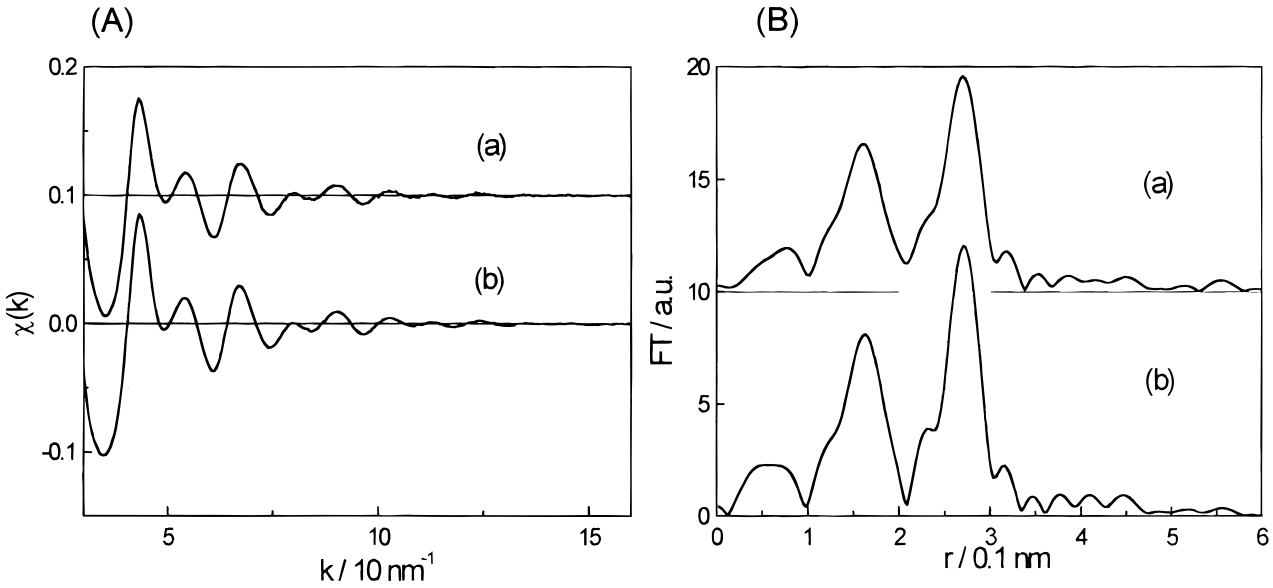

Figure 6. EXAFS oscillations (A) and Fourier transforms (B) of the k^3-weighted EXAFS for 1-$Mo(CO)_6$/NaY (a) and $Mo(CO)_6$ powder (b).

TABLE 3: Curve-Fitting Results of 1-$Mo(CO)_6$/NaY[a]

	pair	*N*	*r*/nm	Δ*E*/eV	σ/nm	R_f/%
$Mo(CO)_6$/NaY	Mo−C	5.8 ± 0.2	0.208 ± 0.001	1.0 ± 1.0	0.0065 ± 0.001	1.0
	Mo−O	6.1 ± 0.2	0.323 ± 0.001	1.4 ± 1.0	0.0064 ± 0.001	0.8
$Mo(CO)_6$	Mo−C	(6.0)	(0.208)	(0.0)	(0.006)	
	Mo−O	(6.0)	(0.323)	(0.0)	(0.006)	

[a] The parentheses indicate the coordination numbers, bond lengths, and Debye−Waller factors used as standard. Δ*E* is the deviation of kinetic energy zero for photoelectron from that of standard compound.

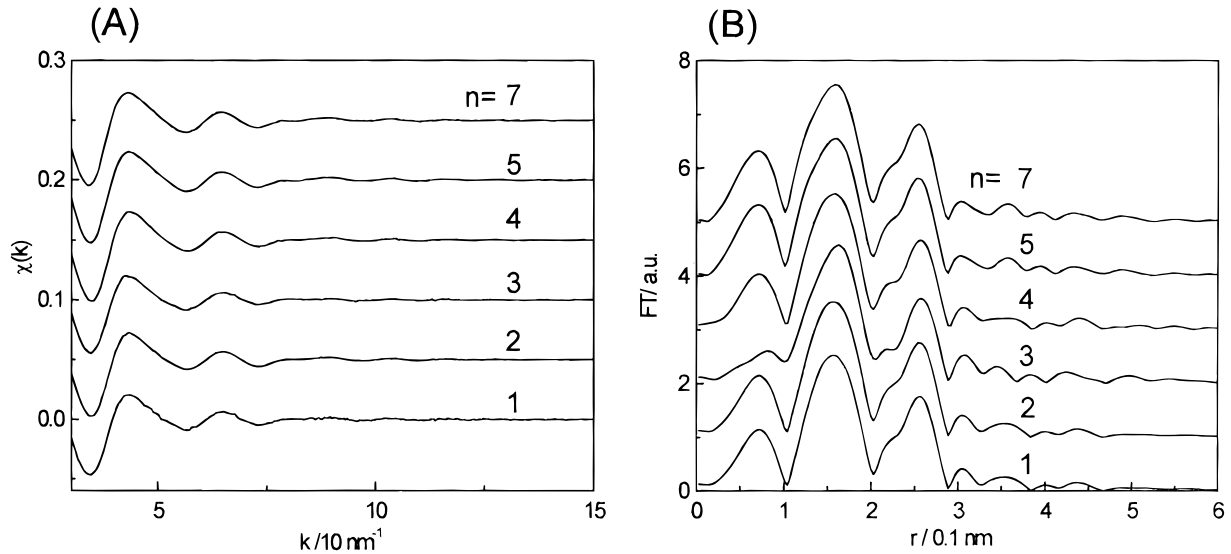

Figure 7. EXAFS oscillations (A) and Fourier transforms (B) of k^3-weighted EXAFS oscillations for Mo(*n*)/NaY(*n* = 1, 2, 3, 4, 5, and 7). The numbers of cycle (*n*) are given in the figure.

transformed to *k* space over 0.1−0.33 nm, and curve-fitting analysis was carried out using the phase-shift and amplitude function derived from the corresponding bonds of $Mo(CO)_6$. The results are given in Table 3. Mo−C and Mo−O were determined to be 0.208 ± 0.001 nm (coordination number 5.8 ± 0.2) and 0.323 ± 0.001 nm (coordination number 6.1 ± 0.2), respectively. The bond distances agree well with those of $Mo(CO)_6$ (Mo−C = 0.208 nm and Mo−O = 0.323 nm), indicating the $Mo(CO)_6$ structure is intact in the NaY.

Figure 7 shows EXAFS oscillations [$\chi(k)$] and Fourier transforms of the $k^3\chi(k)$ for Mo species after the *n* cycles of saturated adsorption−thermal decomposition processes (*n* = 1, 2, 3, 4, 5, and 7). Two peaks assigned to Mo−O and Mo−Mo appeared in the Fourier transform. All the EXAFS oscillations were identical, independent of the number of cycles, indicating that the local structures around Mo atoms in the zeolite pores were almost the same for all the samples prepared by the CVD method.

To confirm this point we analyzed the data by χ^2 test using the following equations.

$$\aleph^2 = [1/(N-2)]\sum[\chi_1(k_i) - \chi_r(k_i)]^2/[\sigma_1(k_i)^2 + \sigma_r(k_i)^2] \quad (4)$$

where $\chi_1(k_i)$ and $\chi_r(k_i)$ are the EXAFS oscillations extracted from

TABLE 4: $\aleph^2$ and Limit of Confidence for $\chi(k)$ Functions of Mo(n)/NaY Calculated by eq 4[a]

sample	$\aleph^2$	probability	no. of freedom
Mo(2)/NaY	0.84	95%	200
Mo(3)/NaY	0.95	69%	200
Mo(4)/NaY	0.85	94%	200
Mo(5)/NaY	0.92	79%	200
Mo(7)/NaY	0.94	71%	200

[a] Mo(1)/NaY was used as a reference oscillation $\chi_r(k)$.

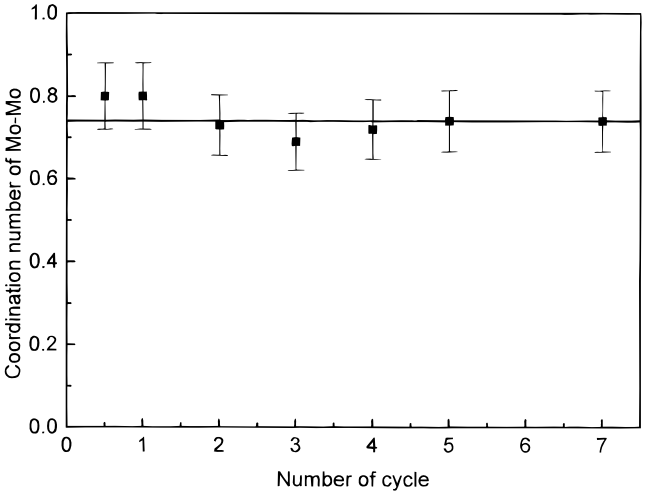

Figure 8. Plots of the Mo−Mo coordination number derived from EXAFS analysis against the number of cycles.

two data sets. N is the number of data points. The $\sigma_1(k_i)^2$ and $\sigma_r(k_i)^2$ were estimated from the standard deviations of the measured data. If we could measure infinite number of data points and $\aleph^2$ were less than unity, one could say the two data sets were identical perfectly. For the data sets with finite number of data points, we can say that two data sets are identical with a certain probability determined by χ^2 distribution with the freedom of N−2. We calculated $\aleph^2$ value using eq 4, taking Mo(1)/NaY as a reference. Table 4 summarizes the $\aleph^2$ values and the probability that the two data sets are identical. The $\aleph^2$ values were less than unity and the probabilities were higher than 69%. Thus we can conclude the majority of Mo species in the NaY supercage are identical for all the Mo(n)/NaY samples (n =1, 2, 3, and 4) independent of the loading.

To obtain the detail of structural information on the decomposed Mo species, we carried out the curve-fitting analysis on the inversely Fourier transformed peaks over 0.1−0.35 nm. We were not able to obtain good fitting results by assuming two shells of Mo−O + Mo−Mo bonds (R factor > 10%). Moreover, the fitted data gave Debye−Waller factor for Mo−O > than 0.01 nm, indicating the presence of large disorder in the first shell due to more than two types of coordination of light elements (O) at different Mo−O distances. Then we carried out three-shell fitting (2 Mo−O + Mo−Mo bonds) and we obtained the best fit results with R factor < 5%, given in Table 5. All the Mo(n)/ NaY samples gave similar fitting results. Observation of Mo−Mo distance argues that Mo ensembles were formed after the thermal decomposition at 573 K. We plotted the coordination number of Mo−Mo against the repetition number of saturated adsorption−thermal decomposition cycles, as shown in Figure 8. As a straight line parallel to the x-axis can be drawn, the Mo−Mo coordination number seems to be constant within the error bar. Thus it is most likely that the nuclearity of the Mo ensembles formed after the decomposition does not vary with the number of saturated adsorption−thermal decomposition cycles.

Figure 9 shows the EXAFS oscillation [$\chi(k)$] and Fourier transforms of $k^3\chi(k)$ for Mo species after oxidation of Mo(1)/NaY at 673 K for 1 h. The sample is denoted as Mo(1,ox)/NaY hereafter. Only one peak due to Mo−O was found at about 0.15 nm, and the second peak originating from Mo−Mo that had been observed in Figure 7 disappeared in Figure 9. The curve-fitting analysis showed the coordination number of 3.6 ± 0.5 and the bond length of 0.173 ± 0.002 nm for Mo−O. These structure parameters are similar to those for tetrahedral MoO_4^{2-} (coordination number = 4 and bond length = 0.176 nm).

X-Ray Absorption Near-Edge Structure (XANES). Figure 10 shows XANES spectra for the $Mo(CO)_6$−CVD samples and reference compounds. XANES spectra were sensitive to the local structure and electronic state of X-ray-absorbing atom(Mo). After the $Mo(CO)_6$ was adsorbed on the supercage of NaY, two distinct peaks appeared at 20 016 and 20 036 eV in Figure 10(a) that were similar to the peaks for $Mo(CO)_6$ crystal [Figure 10-(e)], indicating the presence of $Mo(CO)_6$ species in the supercage. After the thermal treatment at 573 K, the peaks disappeared, indicating that the $Mo(CO)_6$ species was decom-

TABLE 5: Curve-Fitting Results of Mo(n)/NaY(n = 1, 2, 3, 4, 5, and 7)

n[a]	pair	N	r/nm	σ/nm	E_0/eV	R_f/%
1[b]	Mo−O	5.5 ± 0.5	0.200 ± 0.002	0.0115 ± 0.004	3.0 ± 3.0	12
	Mo−Mo	0.8 ± 0.3	0.284 ± 0.003	0.0075 ± 0.0015	4.8 ± 3.0	
1	Mo−O(C)[c]	1.3 ± 0.4	0.195 ± 0.002	0.0076 ± 0.0015	1.4 ± 2.0	
	Mo−O	1.1 ± 0.4	0.210 ± 0.003	0.0079 ± 0.0015	0.0 ± 2.0	2
	Mo−Mo	0.8 ± 0.3	0.284 ± 0.003	0.0080 ± 0.0015	4.8 ± 3.0	
2	Mo−O(C)[c]	1.3 ± 0.4	0.195 ± 0.003	0.0078 ± 0.002	1.2 ± 2.0	
	Mo−O	1.0 ± 0.4	0.210 ± 0.003	0.0079 ± 0.0015	−0.5 ± 2.0	3
	Mo−Mo	0.7 ± 0.3	0.285 ± 0.003	0.0082 ± 0.002	3.3 ± 3.0	
3	Mo−O(C)[c]	1.2 ± 0.4	0.194 ± 0.002	0.0075 ± 0.002	1.0 ± 2.0	
	Mo−O	1.0 ± 0.4	0.210 ± 0.003	0.0081 ± 0.002	1.5 ± 2.0	3
	Mo−Mo	0.7 ± 0.4	0.286 ± 0.004	0.0079 ± 0.002	5.0 ± 4.0	
4	Mo−O(C)[c]	1.4 ± 0.4	0.196 ± 0.002	0.0077 ± 0.003	1.3 ± 3.0	
	Mo−O	1.2 ± 0.4	0.211 ± 0.002	0.0081 ± 0.002	2.8 ± 3.0	3
	Mo−Mo	0.7 ± 0.3	0.285 ± 0.003	0.0075 ± 0.002	4.0 ± 3.0	
5	Mo−O(C)[c]	1.2 ± 0.4	0.197 ± 0.002	0.0078 ± 0.002	2.0 ± 3.0	
	Mo−O	1.1 ± 0.4	0.211 ± 0.002	0.0079 ± 0.003	3.5 ± 3.0	2
	Mo−Mo	0.8 ± 0.4	0.285 ± 0.003	0.0075 ± 0.002	4.0 ± 4.0	
7	Mo−O(C)[c]	1.2 ± 0.4	0.197 ± 0.002	0.0078 ± 0.002	2.8 ± 2.0	
	Mo−O	1.1 ± 0.4	0.208 ± 0.002	0.0081 ± 0.002	3.1 ± 2.0	2
	Mo−Mo	0.7 ± 0.3	0.285 ± 0.003	0.0079 ± 0.002	3.8 ± 3.0	

[a] n is the number of saturated adsorption−thermal decomposition cycles. [b] One-term fitting for the first shell of Mo(1)/NaY. [c] The comprehensive data suggest the presence of M−C bonds.

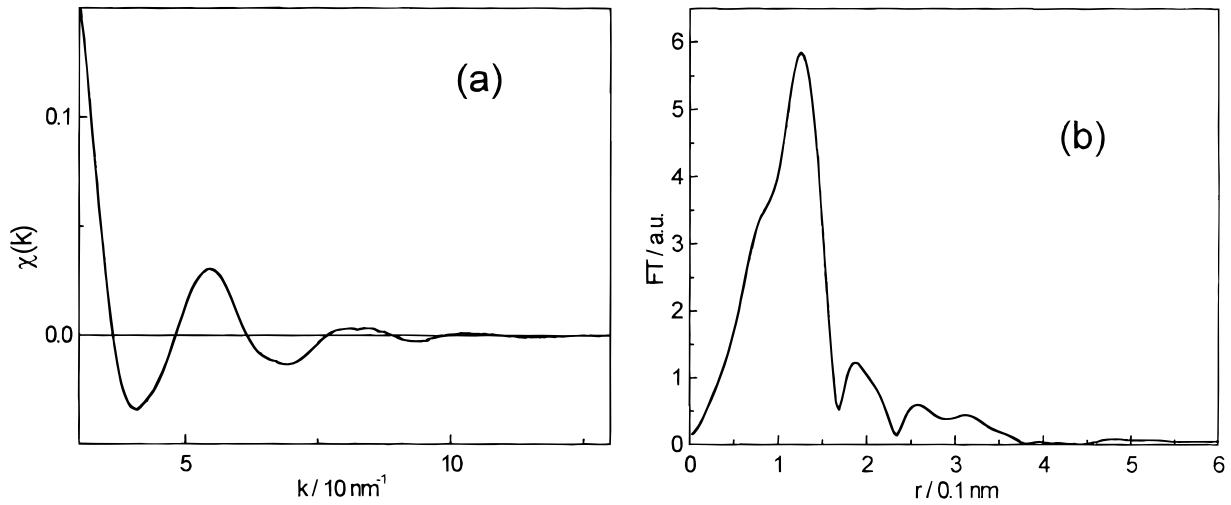

Figure 9. EXAFS oscillation (a) and Fourier transforms (b) of the k^3-weighted EXAFS oscillations for Mo(1,ox)/NaY after oxidation with O_2 at 673 K.

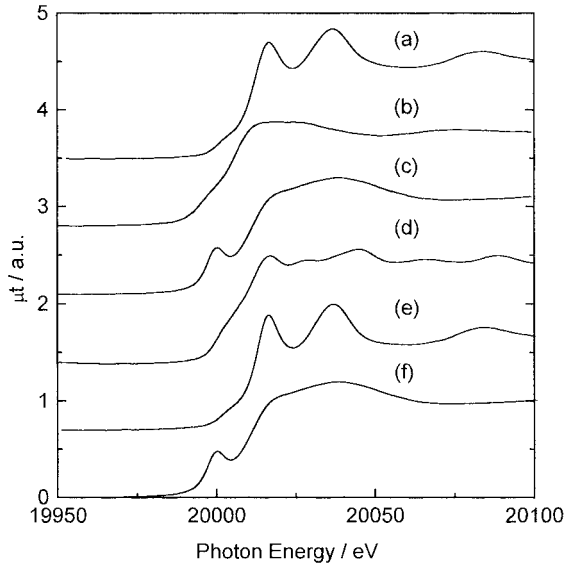

Figure 10. XANES spectra for 1-$Mo(CO)_6$/NaY (a), Mo(1)/NaY (b), subsequent oxidation at 673 K (c), Mo foil (d), $Mo(CO)_6$ (e), and K_2MoO_4 (f).

posed. Figure 10(c) shows the XANES spectrum for the Mo-(1,ox)/NaY after oxidation of the treated sample at 673 K. The preedge peak assigned to the Mo 1s → 4d transition clearly appeared at the preedge. The strong 1s → 4d peak suggests that the Mo species has a tetrahedral symmetry. In fact, K_2MoO_4, which has a tetrahedral structure, shows the strong 1s → 4d peak at the same position as the Mo(1,ox)/NaY.

Discussion

Structure of $Mo(CO)_6$ inside NaY Supercage. Conventional impregnation using an aqueous solution of ammonium heptamolybdate results in Mo supported mainly at the external surface because oxoanionic or neutral complexes hardly penetrate into zeolite pores in the presence of water.[32] On the other hand, Mo-$(CO)_6$ and $W(CO)_6$ are often used as precursors to immobilize Mo and W species inside the pores. The size of $Mo(CO)_6$ is about 0.75 nm, which is a little larger than the channel of NaY zeolite (0.74 nm) and smaller than the pore size of the supercage of NaY(1.2 nm). The maximum Mo loading after one saturated adsorption of $Mo(CO)_6$ is determined to be two per supercage, agreeing with the literature.[13,20,25] XPS studies show that the Mo $3d_{5/2}$ peak intensity relative to the Si 2p peak intensity was 0.32, which is smaller than that for the $(NH_4)_6Mo_7O_{24}$ impregnated sample, in which $Mo_7O_{24}^{6-}$ is located mainly at the external surface of NaY. Thus it is likely that Mo species derived from $Mo(CO)_6$ is located in the supercages. The size of supercages is as large as or a little smaller than the sum of diameter of two $Mo(CO)_6$ molecules. The adsorbed $Mo(CO)_6$ may be closely packed inside the supercage. Previous FT-IR and Na−NMR indicated that the $Mo(CO)_6$ interacted with Na^+ ions at site II and was deformed to C_{2v} symmetry.[23,24,33] Present EXAFS analysis shows that the bond lengths and coordination numbers of Mo−C and Mo−O in $Mo(CO)_6$ /NaY are almost the same as those for unsupported $Mo(CO)_6$. Distortion of the adsorbed $Mo(CO)_6$ in NaY seems to be less than the detection limit of EXAFS. XANES spectra have been demonstrated to be sensitive to symmetry change.[34] However, the spectra of unsupported $Mo(CO)_6$ and $Mo(CO)_6$ adsorbed in NaY were almost the same, as shown in Figure 10. From XANES and EXAFS, we cannot obtain evidence for distortion of $Mo(CO)_6$ molecules trapped in the supercage of NaY.

Structure after Decomposition. TPD spectra in Figure 2 revealed that almost all carbonyls in adsorbed $Mo(CO)_6$ desorb before 573 K. Okamoto et al. reported that the total number of the desorbed CO up to 573 K was six per $Mo(CO)_6$ species in the TPD spectra with a ramping speed of 1.8 K/min and two peaks around 380 and 470 K.[15] They assigned the former peak as desorption of three carbonyls to form $Mo(CO)_3$ species. We have found only one TPD peak at 473 K in Figure 1, probably due to the different ramping rates between the two experiments (1.8 K min against 4 K/min). Another difference was observed with the total number of CO desorbed during TPD, which was about 5.5 in our work, indicating that 0.5 carbon atom was left after the thermal decomposition of adsorbed $Mo(CO)_6$. The presence of carbon in the treated samples was also confirmed by the formation of CO_2 by oxidation of the samples after the TPD. The carbon atoms may be associated with the Mo species because the number of carbon atoms left after the thermal decomposition is always close to 0.5 per Mo in the Mo(n)/NaY (n = 1, 2, and 3) samples. In the EXAFS curve fitting analysis we can reproduce the EXAFS oscillation well with the three-shell model composed of two different bonds at 0.195 nm and 0.210 nm for the first shell and the bond at 0.285 nm for the second shell due to Mo−Mo. One of the observed bond distances for the first shell may be tentatively assigned to the

carbon atoms directly bound to the Mo ensemble to form a Mo oxocarbide species. The previous EXAFS work on Mo species on SiO_2 and Al_2O_3 demonstrated Mo−O distances of 0.203−0.210 nm.[35] Thus the longer bonding (0.210 nm) can be attributed to Mo−O-X (X = Si or Al), whereas the shorter one at 0.195 nm may be due to Mo−C. The Mo $3d_{5/2}$ binding energies in the XPS spectra for Mo(*n*)/NaY (*n* = 1, 2, and 3) after thermal decomposition are about 228.8 eV (Table 2). The binding energies are higher than Mo metal foil but lower than MoO_2 (Table 2). Okamoto et al.[15] and Andersson and Howe[16] reported the binding energies of Mo $3d_{5/2}$ level (228.2−229.2 eV) for Mo/NaY obtained by thermal decomposition of Mo-$(CO)_6$ NaY in vacuo at 473−673 K, as shown in Table 2. On the basis of the observed binding energies, they concluded that the small metallic aggregates (zero-valent Mo) were created in the pore,[15,16] where slightly larger binding energies of the sample than that of Mo metal were thought to be due to the size effect of small Mo aggregates.[16] However, the present EXAFS results as well as the previous ones[17] suggest the presence of Mo−O bonds and hence the positively charged Mo species. XANES and EXAFS data revealed that Mo(1,ox)/NaY have tetrahedral MoO_4^{2-} structure with Mo^{6+} ions. Two oxygen uptake per Mo in the oxidation of Mo(1)/NaY at 673 K as shown in Table 1 indicates that the Mo species in the thermally decomposed Mo-(1)/NaY are in a divalent state. The Mo(*n*)/NaY(*n* = 1, 2, 3, 4) samples after the thermal decomposition showed Mo−Mo bond at 0.285 nm with the coordination number of ∼0.7, independent of the Mo loading, as shown in Figure 8. We propose a dimer structure as a main Mo species in the NaY supercages based on the coordination number of Mo−Mo. This dimer model is rationalized by the following consideration. Two $Mo(CO)_6$ molecules can be immobilized in all supercages at saturation as shown in Figure 1. Linear increase of Mo quantity against the number of saturated adsorption−thermal decomposition cycles in Figure 3 indicates homogeneous distribution of the deposited Mo species throughout the supercages in NaY and little migration of the Mo species during the thermal treatment at 573 K. These results demonstrate that only two Mo^{2+} species are present in a supercage after thermal decomposition of Mo-$(CO)_6$ at 573 K. Thus Mo dimer is a most plausible candidate for the Mo species in the thermally decomposed Mo(1)/NaY samples. We studied structures of Mo^{2+} dimers on SiO_2 derived from $Mo_2(C_3H_5)_4$ by EXAFS[35] and found that Mo−Mo distances ranged from 0.25 to 0.28 nm, depending on the kind of SiO_2 supports. As shown in Table 5, the Mo−Mo distance of the Mo dimers in the NaY zeolite is 0.284 nm, which is similar to those for the Mo dimers attached on SiO_2. As a summary we propose a Mo oxocarbide dimer structure $Mo_2(C)O_x$ with Mo−O and Mo−C at 0.210 nm and 0.195 nm, respectively, for the Mo species in the thermally treated Mo(1)/NaY.

Structure of Mo Species after Adsorption and Decomposition Processes. It was found that two $Mo(CO)_6$ molecules can be further loaded inside the supercage, which already possessed the decarbonylated Mo oxocarbide dimer species. The number of the adsorbed $Mo(CO)_6$ in a supercage linearly increased by two $Mo(CO)_6$ per one cycle of saturated adsorption−thermal decomposition and was saturated with eight Mo per supercage after four repetitions of the above process. This linear increase of Mo loading with the repetition of the saturated adsorption−thermal decomposition process and the clear saturation feature at four repetitions of the process suggest that the Mo species homogeneously occupies the supercages of NaY. It is likely that migration of Mo species leading to heterogeneous distribution of Mo species without the formation of $Mo_2(C)O_x$ did not contribute to the observed event under the present preparation conditions. This finding is in contrast to the result of Yong and Howe.[13] They reported that the number of $Mo(CO)_6$ uptake in a supercage in the deposition process, including decomposition at 673 K, higher than the present temperature, neither showed linear increase with the deposition cycle nor saturation loading of Mo species. They found that 20 Mo atoms per supercage were deposited after 14 cycles of adsorption−decomposition on which 0.55 $Mo(CO)_6$ per supercage could still adsorb. This may be due to inhomogeneous distribution of Mo species by migration of Mo species, as demonstrated by EXAFS.[17] We have treated the samples at the lower temperature (573 K), where migration of Mo species is regarded to be negligible.

The detailed analysis of the EXAFS spectra for Mo(*n*)/NaY revealed the identical structures for the Mo oxocarbide dimer species $Mo_2(C)O_x$, irrespective of the number of saturated adsorption−thermal decomposition cycles. The $Mo_2(C)O_x$ species seems to be stable at 573 K and not to aggregate to larger Mo clusters though more than two Mo atoms are present in a supercage. Post-adsorbed $Mo(CO)_6$ reacts with hydroxyls in supercages rather than with the preloaded $Mo_2(C)O_x$ species as demonstrated by EXAFS, which showed the formation of Mo−O bonds accompanied with one Mo−Mo bond formation (Table 5). Formation of $Mo_2(CO)_x$ species in NaY by thermal decomposition of adsorbed $Mo(CO)_6$ at 373 K has been claimed on the basis of IR observation,[12,13] but it has not been evidenced by EXAFS and ESR.[36,22] Two $Mo(CO)_6$ molecules in the NaY supercage are compressed by spatial restriction of the supercage, which may promote the formation of Mo dimers. Bond arrangement around Mo atoms in the supercage may also prevent the $Mo_2(C)O_x$ species from aggregation to a larger cluster.

Another interesting point to be mentioned is that no further $Mo(CO)_6$ can be immobilized in the Mo(4)/NaY with eight Mo atoms in a supercage, whereas the Mo(4)/NaY still has empty space for one $Mo(CO)_6$ in the supercage. But even one Mo atom was unable to be deposited on the Mo(4)/NaY, as shown in Figure 3. It may be inferred that two $Mo(CO)_6$ molecules are necessary for the fixation of Mo species in the supercage, probably because one $Mo(CO)_6$ is removed by evacuation at room temperature before decomposition at 573 K.

In conclusion, the Mo dimer species homogeneously distributed in the NaY supercage can be synthesized using $Mo(CO)_6$ as a precursor and cycles of saturated adsorption−thermal decomposition at 573 K. The maximum Mo loading by the present preparation method is eight Mo atoms in a supercage. The EXAFS and O_2 uptake data assume the formation of Mo-(II) oxocarbide $Mo_2(C)O_x$ with the Mo−Mo distance of 0.280 nm as major stable species in the NaY supercage.

Acknowledgment. This work has been supported by CREST (Core Research for Evolutionary Science and Technology) of Japan Science and Technology Corporation (JST). The XAFS measurements have been done with the approval of Photon Factory Advisory Committee (PAC) (proposal no. 96G179).

References and Notes

(1) Thomas, J. M.; Thomas, W. J. *Principles and Practice of Heterogeneous Catalysis*; VCH: Weinheim, 1997.

(2) Zakharov, V. Y.; Zakharova, O. M.; Romanovsky, B. V.; Mardaleishvili, R. E. *React. Kinet. Catal. Lett.* **1977**, *6*, 133.

(3) Montovani, E.; Palladirio, N.; Zanotti, A. *J. Mol. Catal.* **1977/1978**, *3*, 385.

(4) Ichikawa, M. *Adv. Catal.* **1992**, *38*, 283.

(5) Sachtler, W. M. H.; Zhang, Z.; Stakheev, A. Y.; Feeley, J. S. In *New Frontier in Catalysis*; Guczi, L., Ed.; Elsevier: Amsterdam, 1992; Vol. 10, p 271.

(6) Kozlov, A.; Asakura, K.; Iwasawa, Y. *Chem. Lett.* **1997**, 313.

(7) Kozlov, A.; Asakura, K.; Iwasawa, Y. *J. Chem. Soc. Faraday Trans.* **1998**, *94*, 809.

(8) McCarthy, T. J.; Marques, C. M. P.; Trevino, H.; Sachtler, W. M. H. *Catal. Lett.* **1997**, *43*, 11.

(9) Howe, R. F.; Davidson, D. E.; Whan, D. A. *J. Chem. Soc. Faraday Trans. I*, **1972**, *68*, 2266.

(10) Smith, J.; Howe, R. F.; Whan, D. A. *J. Catal.* **1974**, *34*, 191.

(11) Howe, R. F. *Inorg. Chem.* **1976**, *15*, 486.

(12) Abdo, S.; Howe, R. F. *J. Phys. Chem.* **1983**, *87*, 1713.

(13) Yong, Y.-S.; Howe, R. F. *J. Chem. Soc. Faraday Trans.* **1986**, *82*, 2887.

(14) Maezawa, A.; Kane, H.; Okamoto, Y.; Imanaka, T. *Chem. Lett.* **1988**, 241.

(15) Okamoto, T.; Maezawa, A.; Kane, H.; Mitsushima, I.; Imanaka, T. *J. Chem. Soc. Faraday Trans. I* **1988**, *84*, 851.

(16) Andersson, S. L. T.; Howe, R. F. *J. Phys. Chem.* **1989**, *93*, 4913.

(17) Coddington, J. M.; Howe, R. F.; Yong, Y.-S.; Asakura, K.; Iwasawa, Y. *J. Chem. Soc. Faraday Trans.* **1990**, *86*, 1015.

(18) Okamoto, Y.; Kobayashi, Y.; Imanaka, T. *Catal. Lett.* **1993**, *20*, 49.

(19) Ozin, G. A.; Ozkar, S. *J. Phys. Chem.* **1990**, *94*, 7556.

(20) Ozkar, S.; Ozin, G. A.; Moller, K.; Bein, T. *J. Am. Chem. Soc.* **1990**, *112*, 9575.

(21) Moller, K.; Bein, T.; Ozkar, S.; Ozin, G. A. *J. Phys. Chem.* **1991**, *95*, 5276.

(22) Okamoto, Y.; Imanaka, T.; Asakura, K.; Iwasawa, Y. *J. Phys. Chem.* **1991**, *95*, 3702.

(23) Jelinek, R.; Ozkar, S.; Ozin, G. A. *J. Phys. Chem.* **1992**, *96*, 5949.

(24) Jelinek, R.; Ozkar, S.; Ozin, G. A. *J. Am. Chem. Soc.* **1992**, *114*, 4907.

(25) Ozin, G.; Ozkar, S.; Prokopowicz, R. A. *Acc. Chem. Res.* **1992**, *25*, 553.

(26) Okamoto, Y.; Kobayashi, Y.; Imanaka, T. *Catal. Lett.* **1993**, *20*, 49.

(27) Ozin, G. A.; Steel, M. R. *Macromol. Symp.* **1994**, *80*, 45.

(28) Djajanti, S. D.; Howe, R. F. In *Zeolites: A Refined Tool for Designing Catalytic Sites*; Bonneviot, L., Kaliaguine, S., Eds.; Elsevier Science: Amsterdam, 1995.

(29) Asakura, K. In *X-ray Absorption Fine Structure for Catalysts and Surfaces*; Iwasawa, Y., Ed.; World Scientific: Singapore, 1996; p 33.

(30) Stern, E. *Phys. Rev. B* **1993**, *48*, 9825.

(31) Cid, R.; Llambias, F. J. G.; Fierro, J. L. G.; Agudo, A. L.; Villasenor, J. *J. Catal.* **1984**, *89*, 478.

(32) Fierro, J. L. G.; Conesa, J. C.; Agudo, A. L. *J. Catal.* **1987**, *108*, 334.

(33) Muller, B. R.; Calzaferri, G. *J. Chem. Soc. Faraday Trans.* **1996**, *92*, 1633.

(34) Kosugi, N. In *X-ray Absorption Fine Structure for Catalysis and Surfaces*; Iwasawa, Y., Ed.; World Scientific: Singapore, 1996; p 60.

(35) Iwasawa, Y. *Adv. Catal.* **1987**, *35*, 187.

(36) Abdo, S.; Howe, R. F. *J. Phys. Chem.* **1983**, *87*, 1722.

(37) Swartz, Jr., W. E.; Hercules, D. M. *Anal. Chem.* **1971**, *43*, 1774.

(38) Ochoa, R.; Bi, X. X.; Rao, A. M.; Eklund, P. C. *The Chemistry of Transition Metal Carbides and Nitrides*; Oyama, S. T., Ed.; Blackie Academic and Professional: London, 1996; p 489.